






## RESEARCH ARTICLE

10.1029/2023GC010947

# Global Hydrogen Production During High-Pressure Serpentinization of Subducting Slabs

A. S. Merdith<sup>1</sup> , I. Daniel<sup>2</sup> , D. Sverjensky<sup>3</sup>, M. Andreani<sup>2</sup>, B. Mather<sup>4</sup> , S. Williams<sup>5</sup>, and A. Vitale Brovarone<sup>6,7,8</sup>

<sup>1</sup>School of Earth and Environment, University of Leeds, Leeds, UK, <sup>2</sup>Laboratoire de Géologie de Lyon, CNRS-INSU, Université Lyon I, Lyon, France, <sup>3</sup>Department of Earth & Planetary Sciences, Johns Hopkins University, Baltimore, MD, USA, <sup>4</sup>School of Geosciences, The University of Sydney, Sydney, NSW, Australia, <sup>5</sup>State Key Laboratory of Continental Dynamics, Department of Geology, Northwest University, Xi'an, China, <sup>6</sup>Dipartimento di Scienze Biologiche, Geologiche e Ambientali (BiGeA), Alma Mater Studiorum Università di Bologna, Bologna, Italy, <sup>7</sup>Institut de Minéralogie, de Physique des Matériaux et de Cosmochimie (IMPMC), Sorbonne Université, Muséum National d'Histoire Naturelle, UMR CNRS 7590, IRD UR206, Paris, France, <sup>8</sup>Institute of Geosciences and Earth Resources, National Research Council of Italy, Pisa, Italy

### Key Points:

- First-order estimate of the gross flux of “slab-serpentinization” and the resulting (possible) hydrogen production (4.2–24 • 10<sup>7</sup> kg of H<sub>2</sub> per annum)
- Seafloor spreading history and ocean basin evolution (prior to subduction) impart the strongest control on slab-serpentinization possibility

### Supporting Information:

Supporting Information may be found in the online version of this article.

### Correspondence to:

A. S. Merdith,  
a.s.merdith@leeds.ac.uk

### Citation:

Merdith, A. S., Daniel, I., Sverjensky, D., Andreani, M., Mather, B., Williams, S., & Vitale Brovarone, A. (2023). Global hydrogen production during high-pressure serpentinization of subducting slabs. *Geochemistry, Geophysics, Geosystems*, 24, e2023GC010947. <https://doi.org/10.1029/2023GC010947>

Received 14 MAR 2023

Accepted 25 JUL 2023

### Author Contributions:

**Conceptualization:** A. S. Merdith, I. Daniel, D. Sverjensky, M. Andreani, A. Vitale Brovarone

**Formal analysis:** A. S. Merdith, I. Daniel, D. Sverjensky, S. Williams, A. Vitale Brovarone

**Funding acquisition:** A. S. Merdith, I. Daniel, D. Sverjensky, A. Vitale Brovarone

**Investigation:** A. S. Merdith, I. Daniel, A. Vitale Brovarone

**Methodology:** A. S. Merdith, B. Mather, S. Williams, A. Vitale Brovarone

**Software:** A. S. Merdith

2023. The Authors. Geochemistry, Geophysics, Geosystems published by Wiley Periodicals LLC on behalf of American Geophysical Union. This is an open access article under the terms of the [Creative Commons Attribution-NonCommercial License](https://creativecommons.org/licenses/by/4.0/), which permits use, distribution and reproduction in any medium, provided the original work is properly cited and is not used for commercial purposes.

**Abstract** Serpentinization is among the most important, and ubiquitous, geological processes in crustal–upper mantle conditions (<6 GPa, <600°C), altering the rheology of rocks and producing H<sub>2</sub> that can sustain life. While observations are available to quantify serpentinization in terrestrial and mid-ocean ridge environments, measurements within subduction zone environments are far more sparse. To overcome this difficulty, we design a methodology to quantify and offer a first-order estimate of the magnitude of “slab-serpentinization” that has occurred over the last 5 Ma within the world’s subduction zones by coupling four discrete tectonic and geophysical datasets—(a) raster grids of relic abyssal peridotite (peridotite exhumed from slow spreading mid-ocean ridges but unaffected by pre-subduction serpentinization) within ocean basins, (b) slab geometry, (c) thermal profiles and a (d) plate-tectonic model. Averaged per year, our results suggest that 4.2–24 • 10<sup>7</sup> kg of H<sub>2</sub> per annum could be generated from “slab-serpentinization” within a subduction zone. Our estimate is 3–4 orders of magnitude lower than what is thought to be produced at mid-ocean ridges, and 1–2 orders of magnitude lower than what could occur through serpentinization at trench flexure and when including possible mantle wedge serpentinization. Higher hydrogen production is correlated most strongly with the spreading history of ocean basins, underlaying the importance of the tectonic history of a slab prior to subduction.

**Plain Language Summary** The fate of most ocean crust formed at mid-ocean ridges is to eventually subduct and be recycled into the mantle. Subduction zones therefore represent a key link between the rocks we see at the surface of the Earth, both in oceans and continents, and the underlying mantle. However, subduction zones are impossible to observe directly and therefore difficult to fully understand the processes that shape them. Here, we designed a framework that coupled a series of discrete data sets to model how the composition of each subducting slab across the globe differs in order to provide an accurate estimate of “slab-serpentinization.” Serpentinization is the process that converts mantle rocks to serpentinite through exposure to water. A by-product of this process is the formation of hydrogen gas. Using our framework, we estimated bulk fluxes of serpentinization in subducting slabs, and the corresponding flux of hydrogen.

## 1. Introduction

The evolution of aqueous fluids during subduction zone metamorphism plays a central role in global cycling of life-essential elements, their redox state, and their return to the Earth’s surface (Manning and Shock, 2013; Schmidt & Poli, 2013; Sverjensky & Daniel, 2020). Based on the chemistry of arc magmas, the redox state of forearc-to-subarc slab (50–100 km depth) fluids has long been considered oxidized and dominated by aqueous fluids released through the dehydration of the subducting slab rich in CO<sub>2</sub> (e.g., Debret & Sverjensky, 2017; Padrón-Navarta et al., 2023; Parkinson & Arculus, 1999; Tumiami & Malaspina, 2019). However, several studies over the last 15 years have highlighted the possibility for more reduced fluids, rich in H<sub>2</sub> and other reduced species, and reduced assemblages to form in subduction zone conditions ranging from forearc to sub-arc depth (e.g., Arai et al., 2012; Boutier et al., 2021; Debret et al., 2022; Ferrando et al., 2010; Galvez et al., 2013; Huang et al., 2017; Kutcherov et al., 2020; Malvoisin et al., 2011; Piccoli et al., 2019; Sachan et al., 2007; Tao et al., 2018;

**Validation:** A. S. Merdith, I. Daniel, D. Sverjensky, M. Andreani, A. Vitale Brovarone

**Writing – original draft:** A. S. Merdith, I. Daniel, S. Williams, A. Vitale Brovarone

**Writing – review & editing:** A. S. Merdith, I. Daniel, D. Sverjensky, M. Andreani, B. Mather, S. Williams, A. Vitale Brovarone

Vitale Brovarone et al., 2017, 2020). Assessing the magnitude of deep H<sub>2</sub> in subduction zones is crucial because the presence of such reduced fluids may strongly affect current models of deep geochemical cycling and could act as a source of energy for the deepest subsurface microbial life (Plümper et al., 2017; Rogers et al., 2023; Vitale Brovarone et al., 2020).

The aqueous alteration of ultramafic rocks, or serpentinization, is a key process in forming H<sub>2</sub> and promoting reducing conditions (Andreani et al., 2013; Janecky & Seyfried, 1986). Serpentinization is readily observed in natural environments: at mid-ocean ridges (e.g., Charlou et al., 2002; Kelley et al., 2005; Liu et al., 2023) and on land (e.g., Barnes et al., 1978; Leong et al., 2021; Leong & Shock, 2020; Miller et al., 2016; Sánchez-Murillo et al., 2014), requiring only peridotite to be exposed to water at crustal-to-upper-mantle conditions (<~6 GPa, <~600°C) (Janecky & Seyfried, 1986). The process has also been recreated within laboratory experiments with both natural and synthetic samples at a range of pressures and temperatures (see recent review by Barbier et al., 2020) and thermodynamic modeling of subduction zones predicts the presence of serpentinite minerals, chiefly antigorite, up to a depth of 6 GPa (Abers et al., 2017; Maurice et al., 2020; Ulmer & Trommsdorff, 1995) (though H<sub>2</sub> could be generated more deeply as olivine reacts with water to form magnetite and H<sub>2</sub>, e.g., Malaspina et al., 2023).

Geological evidence of serpentinization within subduction zones is more sparse, despite geophysical evidence suggesting it could affect substantial volumes of convergent margins (Blakely et al., 2005; Bostock et al., 2002; Ranero et al., 2003; Williams & Gubbins, 2019). Above subducting slabs, serpentinization may affect the so-called “cold-nose” of the fore-arc mantle wedge (Abers et al., 2017; Blakely et al., 2005; Bostock et al., 2002; Debret et al., 2022; Fryer, 1996; Hyndman & Peacock, 2003; Mottl et al., 2003; Ohara et al., 2012; Plümper et al., 2017; Vitale Brovarone et al., 2020). Within subducting slabs, serpentinization may take place by trench flexure (e.g., Faccenda, 2014; Ranero et al., 2003), or deeper in subduction zones through the interaction between metamorphic fluids and relic (or residual) abyssal peridotite (RAP)—i.e. peridotite that was exhumed, but not fully serpentinized, at slow spreading ridges and is transported via seafloor spreading to subduction zones and undergoes serpentinization during subduction (Figure 1c, Boutier et al., 2021; Vitale Brovarone et al., 2020).

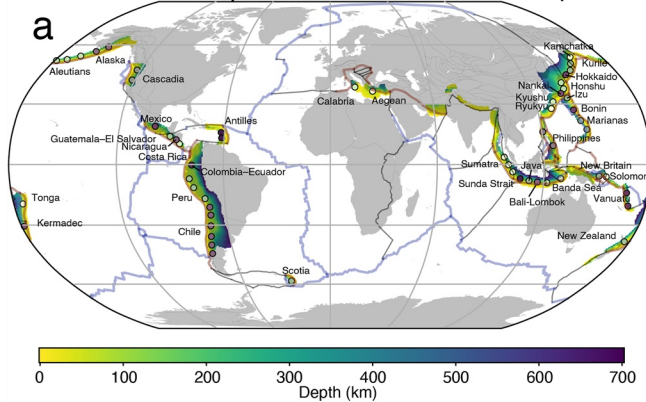
This process of “slab-serpentinization” in the upper most 7 km of the subducting slab (corresponding to the alteration depth of thinned crust at mid-ocean ridges, e.g., Cannat et al., 2010; Merdith et al., 2020) is directly constrained by the raw volume of reactant (i.e., RAP) available, and the pressure-temperature conditions of a subduction zone that control the breakdown of hydrous minerals. For this study, we are interested in the “slab-serpentinization,” which is defined by the pressure-temperature stability curve of antigorite, the highest-temperature serpentinite mineral stable at high-pressure conditions in subduction zones (e.g., Evans, 2004; Schwartz et al., 2013). While some estimates of serpentinization exist from hydration of the forearc mantle wedge (e.g., Carlson & Miller, 2003; Hyndman & Peacock, 2003; Williams & Gubbins, 2019), the presence and extent of slab-serpentinization within subduction zones remain much more speculative (e.g., Vitale Brovarone et al., 2017). Consequently, there is currently no volumetric estimate of possible slab-serpentinization within subduction zones or of the resulting hydrogen flux.

In this study, we approach the problem by coupling discrete data sets including slab geometry (Hayes et al., 2018), thermal profiles (Syracuse et al., 2010) and subduction histories of the world's subduction zones (Müller et al., 2016) (Figures 1a and 1b; Figures S1–S3 in Supporting Information S1). We do this to generate estimates of the global amount of RAP entering subduction zones as part of the subducting oceanic lithosphere (Merdith et al., 2019, 2020). Assuming the sufficient availability of aqueous fluids in the subducting plate (e.g., Faccenda, 2014; van Keken et al., 2011), we estimate the global volume of slab serpentinization and resulting hydrogen production, arising from the upper 7 km of the subducting slab. Our analysis does not consider serpentinization of the mantle wedge and deliberately excludes possible serpentinization of the lithospheric mantle due to trench flexure, the later process which may lower the amount of available RAP for slab-serpentinization, but promote additional serpentinization and H<sub>2</sub> production at convergent margins.

## 2. Overview of Our Approach

Recently, a number of studies have developed techniques to map features forward in time, from ocean basins onto subducted slabs (Harmon et al., 2019; Hicks et al., 2022; McGirr et al., 2021). Here we extend the approach of McGirr et al. (2021) by forward propagating time-sensitive rasterized-grids of different ocean crust properties

Subducted slab depth and locations of thermal profiles



Residual abyssal peridotite

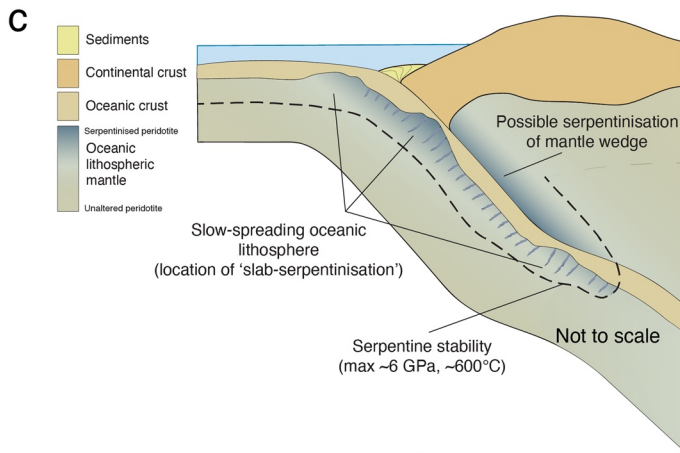
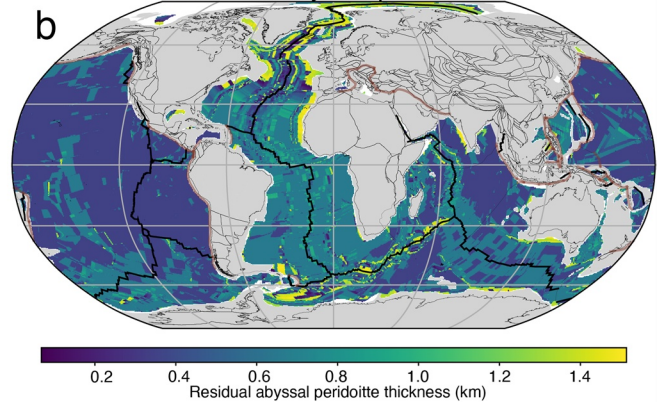


**Figure 1.** (a) Map of Slab2 and Syracuse et al. (2010) data sets. Each circle represents a sample site of thermal properties from Syracuse et al. (2010). (b) Residual abyssal peridotite grid at 0 Ma after Merdith et al. (2019, 2020); (c) Schematic diagram of a subduction zone highlighting “slab-serpentinization” relative to other established settings of serpentinization at subduction zones.

(e.g., seafloor age, RAP content) into a subduction zone (Figure 2, see Supporting Information for more details). We do this forward propagation using the kinematic history of the ocean basins modeled with full-plate reconstructions (models that explicitly model the kinematic evolution of tectonic plates and plate boundaries, e.g., Seton et al. (2023)) to estimate the forward evolution of an ocean plate once it intersects a modeled subduction zone and begins subducting.

We begin our analysis 5 Ma ago to limit our study to the times when the subduction history of the plate model (Müller et al., 2016) is best constrained, though in principle the method could be applied to earlier times. At the start time (i.e., 5 Ma), we extract the velocity orientation and convergence rate of a subducting plate at equally spaced points (latitude, longitude) along the subduction zone. Each point is also used to extract relevant tectonic parameters from our seafloor grids (where they intersect with the subduction zone), including RAP content, seafloor spreading rate at the formation and age of oceanic crust (in principle, any feature intersecting a subduction zone can be used in our method). At each point, we then calculate a dip angle following Mather et al. (2023), who approximate dip based on a range of subducting and over-riding plate properties including age, thickness, buoyancy and rollback (Hu & Gurnis, 2020). The equally spaced points along the subduction zone, therefore, represent the initiation of a *hypothetical subduction isochron*—a line drawn along a subducting slab representing the same time of subduction (e.g., Figure 2, analogous to a seafloor spreading isochron). We can then calculate, using these parameters, the position of the points (latitude, longitude, and depth, using dip angle) and intersected tectonic features after 1 Ma (i.e., 4 Ma ago). We repeat this process for new points intersecting subduction zones, using the new trench-values of orientation, convergence rate and dip to propagate both the new

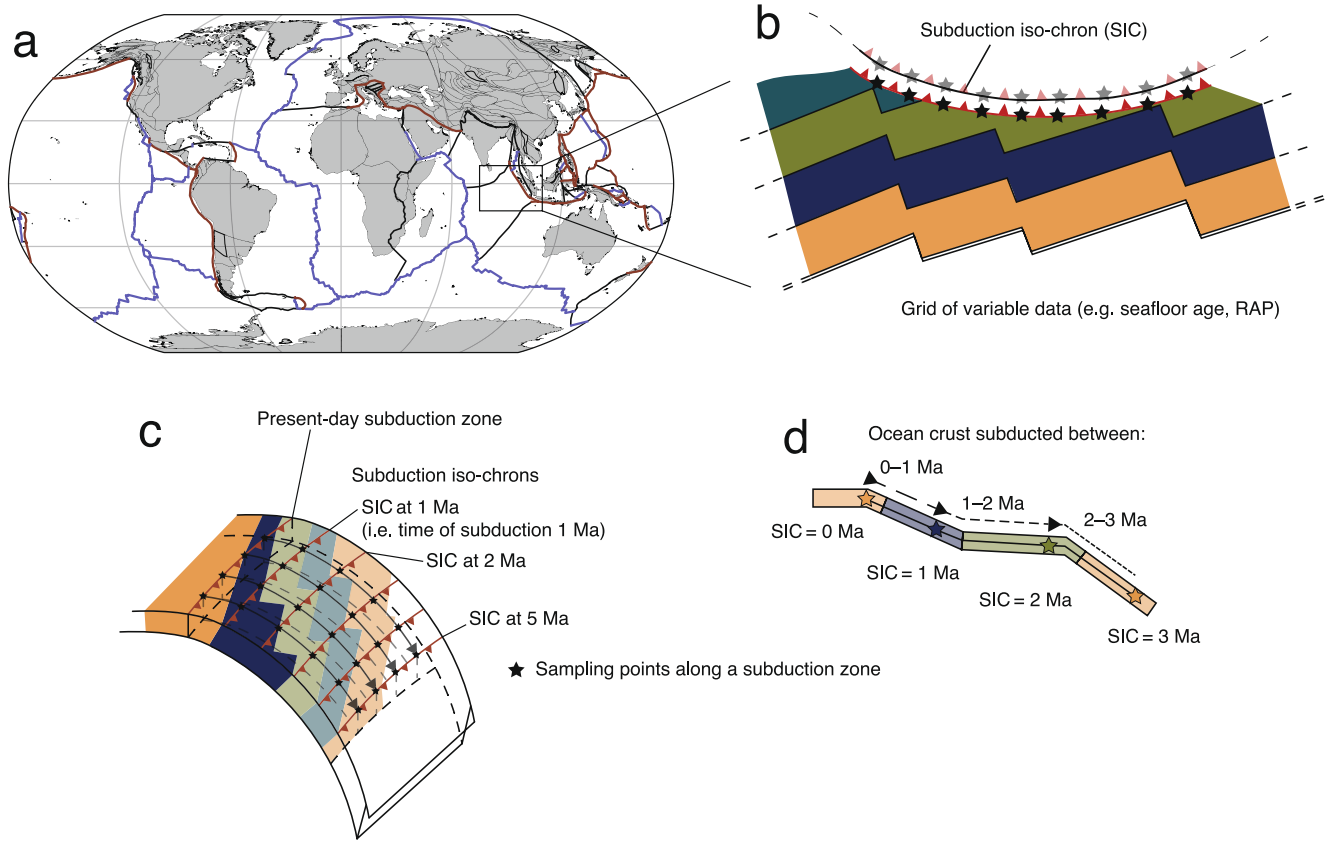


**Figure 2.** Schematic summary of our approach. (a) Plate tectonic model at 0 Ma, highlighting plate boundaries. (b) Sampling at regular intervals across a subduction zone, with artificial isochrons highlighted (the black stars represent the points we sample the hypothetical ocean-basin raster before subduction). (c) Block diagram of a subduction zone showing “subduction isochrons” which the points we subduct represent. (d) As in (c), but a cross section view.

points as well as the previously “subducted” points, forward. This process is repeated until we reach the end time (in this analysis at 0 Ma).

To generate some idea of uncertainty on our method and calculation, we also performed the analysis without correcting for dip. For this second analysis, we also calculated distance from the present-day trench for each point at 0 Ma once the analysis had finished (i.e., based on the convergence rate how far has each point moved since it was “subducted”). We then used this distance to calculate the corresponding depth in the Slab2 geometry based on the distance along the slab surface from the present-day trench. This approach assumes that in the shallow parts of the subduction zones over 1 Ma timescales, slab motion is accounted for by the motion of the downgoing plate.

In order to match our points with the thermal profiles of Syracuse et al. (2010) (SYR10, Figure 1a), we find the nearest geographic profile to each of our subducted points. Because each point that we have subducted contains a “depth” estimate (either through our dip approximating, or directly associating distance from trench to depth along a Slab2 profile), we extract the temperature from the corresponding SYR10 profile at the corresponding depth of our subducted point at the slab Moho (i.e., the temperature between the slab-crust and slab-mantle). Finally, we calculated lithostatic pressure at the modeled point depth.

### 3. Results

Figure 3 displays the sum of all RAP subducted in the last 5 Ma, with the antigorite stability field depicted at varying pressure-temperature conditions (orange line, Figure 3a). Our results are presented in three formats, first with respect to the total amount of RAP subducted over the last 5 Ma (blue circles in Figure 3b), second, with the RAP that sits within the antigorite stability field at present-day (red circles with black outlines in Figure 3b),



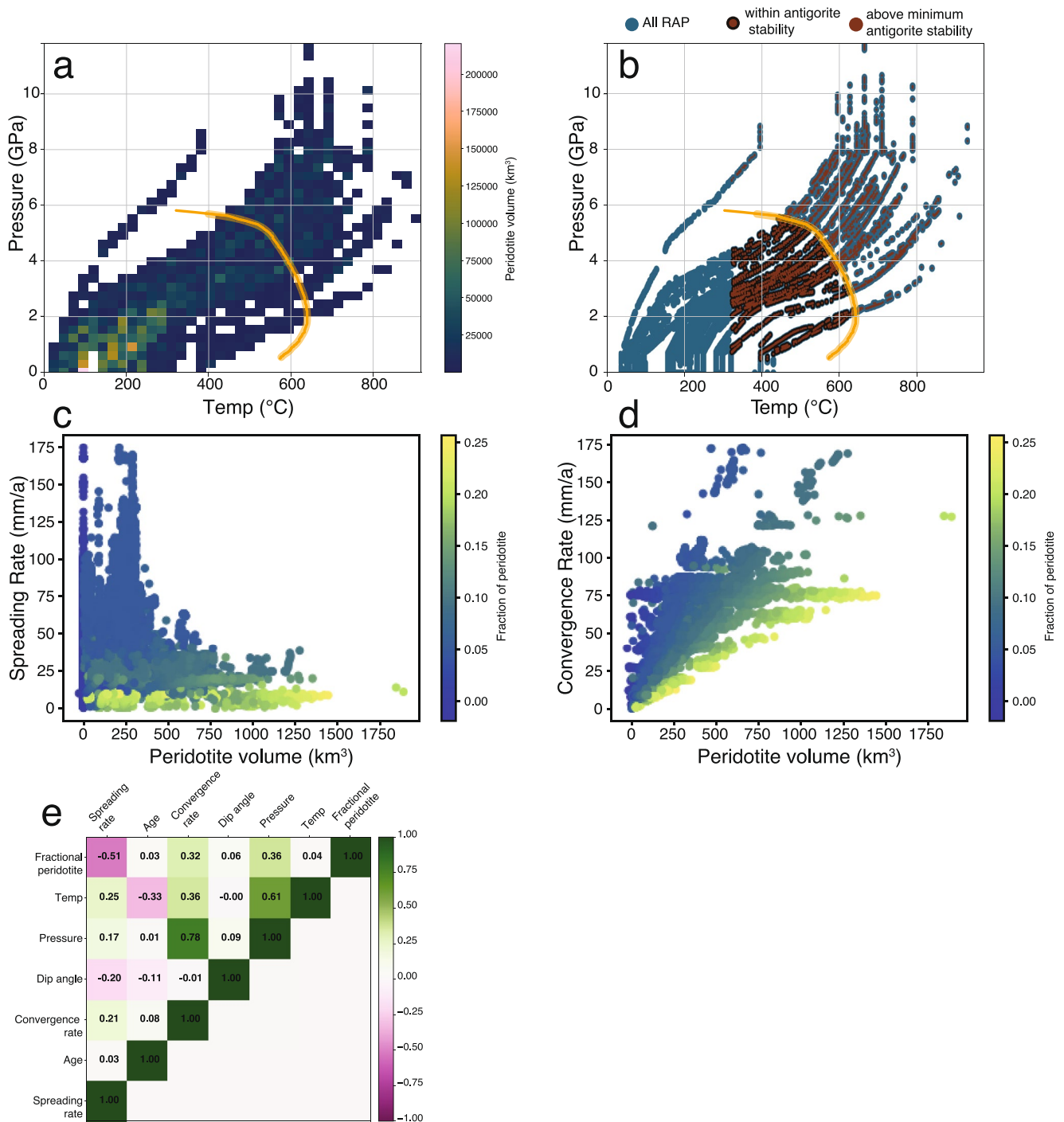


**Figure 3.** Summary of results, (a, b) distribution of RAP in global subduction zones within the antigorite stability field (orange line approximates the lower stability band of antigorite (Schwartz et al., 2013)). Scatterplots highlighting the relationship between the volume of peridotite in subduction zones with spreading rate (c) and convergence rate (d). (e) Pearson correlation coefficient matrix for tectonic parameters—fractional peridotite refers to the fraction of the upper 7 km of the slab that is RAP and the conversion of peridotite mass to hydrogen production is linear. Results use a representative H<sub>2</sub> production value of 200 g per m<sup>3</sup> of reactant.

and finally, with respect to the amount of RAP that sits within, or has passed through, the antigorite stability field at present-day (i.e., including RAP that has been subducted past the upper stability of antigorite, all red circles (including those with black outlines) in Figure 3b).

We calculate a total RAP volume subducted in the last 5 Ma of  $9.2 \cdot 10^6$  km<sup>3</sup> (Figure 3a), with approximately 7%–20% of this volume ( $7$ – $18 \cdot 10^5$  km<sup>3</sup>) currently located within the antigorite stability field (Figure 3a, orange

**Table 1**

Summary of Results of Total Fluxes of RAP Being Subducted and Possible Hydrogen Generation Through Serpentinization

RAP	All subducted RAP (all points in Figure 3b)			Currently within antigorite stability (red points with black outlines in Figure 3b)			Above minimum antigorite stability (0.5 GPa, 320°C, red points in Figure 3b)		
	Moles	Volume (km <sup>3</sup> )	Mass (kg)	Moles	Volume (km <sup>3</sup> )	Mass (kg)	Moles	Volume (km <sup>3</sup> )	Mass (kg)
Per 5 Ma	9.2 • 10 <sup>6</sup>	3.0 • 10 <sup>19</sup>	3.0 • 10 <sup>19</sup>	7–18 • 10 <sup>5</sup>	2.3–6.0 • 10 <sup>18</sup>	2.3–6.0 • 10 <sup>18</sup>	2.3–4.1 • 10 <sup>6</sup>	7.7–13 • 10 <sup>18</sup>	7.7–13 • 10 <sup>18</sup>
Average per annum	1.8	6.1 • 10 <sup>12</sup>	6.1 • 10 <sup>12</sup>	0.13–0.36	5–12 • 10 <sup>11</sup>	5–12 • 10 <sup>11</sup>	0.5–0.8	1.5–2.7 • 10 <sup>12</sup>	1.5–2.7 • 10 <sup>12</sup>
H <sub>2</sub> Per 5 Ma	4.1–14 • 10 <sup>14</sup>	8.3–28 • 10 <sup>14</sup>	8.3–28 • 10 <sup>14</sup>	3.1–27 • 10 <sup>13</sup>	6.2–54 • 10 <sup>13</sup>	6.2–54 • 10 <sup>13</sup>	1.0–6.0 • 10 <sup>14</sup>	2.1–12 • 10 <sup>14</sup>	2.1–12 • 10 <sup>14</sup>
Average per annum	8.2–27 • 10 <sup>7</sup>	1.7–5.5 • 10 <sup>8</sup>	1.7–5.5 • 10 <sup>8</sup>	6.1–54 • 10 <sup>6</sup>	1.2–11 • 10 <sup>7</sup>	1.2–11 • 10 <sup>7</sup>	2.1–12 • 10 <sup>7</sup>	4.2–24 • 10 <sup>7</sup>	4.2–24 • 10 <sup>7</sup>
Fraction of total			0.07–0.2						0.25–0.44

bounds, Figure 3b). However, this estimate omits RAP that has already passed through the antigorite stability field. Including these (now) more deeply subducted sources (red points, Figure 3b), the gross flux of RAP that underwent serpentinization to antigorite is 2.3–4.1 • km<sup>3</sup> over the last 5 Ma; this represents 25%–44% of all subducted RAP and gives an averaged flux of 0.5–0.8 km<sup>3</sup> per annum (Table 1).

To calculate hydrogen production, we follow the approach of Vitale Brovarone et al. (2020), who suggested that 90–300 g of H<sub>2</sub> is produced per 1 m<sup>3</sup> of reactant peridotite assuming ~50% serpentinization and a fluid-rock ratio of 1:1 (figures are produced using a representative value of 200 g per 1 m<sup>3</sup>, see SI for further details). This method yields a total hydrogen production (from peridotite within and that has passed through the antigorite stability field at present-day) of 2.1–12 • 10<sup>14</sup> kg (1.0–6.0 • 10<sup>14</sup> mol) of H<sub>2</sub>, roughly 4.2–24 • 10<sup>7</sup> kg (2.1–12 • 10<sup>7</sup> mol) of H<sub>2</sub> per annum. A “present-day” flux based on our modeled RAP currently within the antigorite stability field is the same order of magnitude, between 1.2 and 11 • 10<sup>7</sup> kg (6.1–54 • 10<sup>6</sup> mol) of H<sub>2</sub>.

To investigate H<sub>2</sub> production within different subduction zones, we isolated the volume of subducted peridotite against both convergence rate (at time of subduction) and spreading rate (at time of seafloor production) (Figures 3c and 3d). As well as calculating a Pearson's Correlation matrix to understand the relationship between various tectonic parameters and the amount of hydrogen formed (which is a linear product of peridotite content) (Figure 3e). Our results indicate that the strongest positive correlation is between peridotite, and pressure or depth and convergence rate (both 0.36 and 0.32 respectively), with the relationship between peridotite volume and convergence rate also clear in Figure 3d. These positive correlations are likely because a high convergence rate results in a larger overall volume of subducted oceanic lithosphere at greater depths. There is a strong negative correlation between spreading rate at the time of formation and fractional peridotite content (–0.51), as expected (also Figure 3c). The correlation between spreading rate and RAP becomes more strongly negative (–0.73) if we consider just the thickness of peridotite being subducted, and more weakly negative (–0.03) if we consider its absolute volume. The reason for the weakening of the correlation when considering the volume of RAP is that currently the majority of subduction occurs around the intermediate–fast spreading Pacific Ocean, thus the absolute volume of crust being subducted outweighs the lower amount of modeled RAP preserved in the crust.

## 4. Discussion

### 4.1. Tectonic Controls on Slab-Serpentinization

Our analysis does not include any estimate of the serpentinization taking place within the seafloor, after mid-ocean ridge serpentinization and before it enters the subduction trench. Therefore, the kinematic conditions of the ridge segment where our subducting lithosphere originally formed exert a first-order control on the amount of available RAP. This is because ocean lithosphere formed at ultra-slow–slow-spreading ridges contains significant volumes of exhumed mantle (e.g., Tucholke & Lin, 1994), and when this lithosphere eventually subducts, there are large volumes of relic peridotite (relative to crust at a fast-spreading ridge) available to be serpentinized within the top 7 km. Broadly, the method we have implemented (Merdith et al., 2020) suggests that on average about 1/3rd of new oceanic lithosphere at a slow–ultraslow spreading ridge are mafic volcanics and 2/3rds are exhumed peridotite, with approximately half of the exhumed peridotite reacting to form serpentinite. This estimate is in line with other estimates of exhumation and serpentinization of mid-ocean ridge peridotites (Cannat et al., 2010; Worman et al., 2016).

The influence of the seafloor spreading history can be seen in a map-view of our results (Figures 4 and 5). For example, the Andean and Izu-Bonin systems produce significantly less H<sub>2</sub> than other subduction zones such as the Philippines or Sumatra. This is a direct consequence of the fact that the seafloor being subducted at the Andean margin formed at an intermediate–fast spreading ridge (Pacific-Farallon ridge, e.g., Seton et al., 2020, 2012) and is unlikely to contain large amounts of exhumed abyssal peridotite. Conversely, in the north-eastern Indian ocean, segments of the ocean crust being subducted under Sumatra formed at a modeled ultraslow–slow ridge (e.g., Jacob et al., 2014), and the volume of peridotite and resulting hydrogen are inferred to be three–four times larger (Figures 4 and 5).

Complementing the seafloor spreading history, the positive correlation between convergence rate and fractional peridotite—the fraction of subducting crust that is comprised of RAP—(and, by extension,

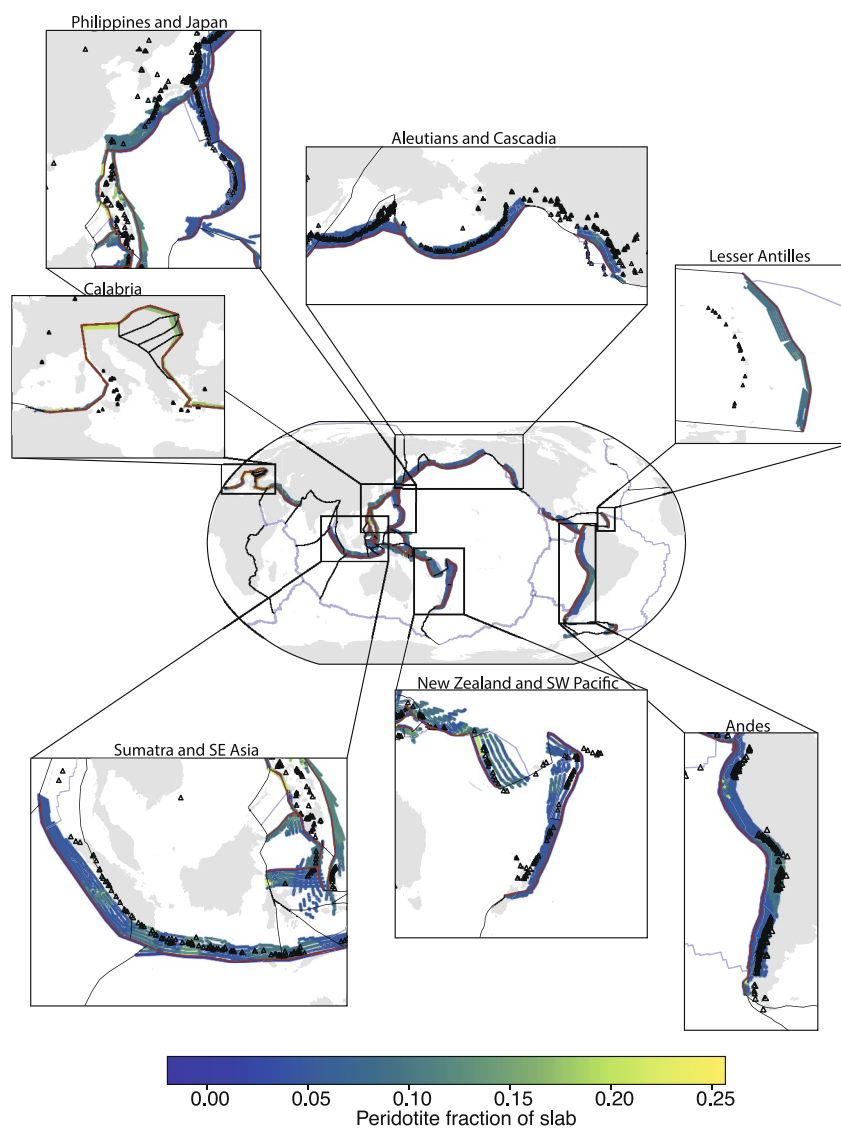


**Figure 4.** Modeled subducted residual abyssal peridotite over the last 5 Ma. Inserts show close-ups of some subduction zones discussed further in text. Holocene volcanoes are plotted on top from the Global Volcanism Project (2023). Global results of other parameters (e.g., fractional peridotite content, depth, dip etc. are available in Supporting Information S1). Results use a representative  $H_2$  production value of  $200 \text{ g per m}^3$  of reactant.

hydrogen production) simply occurs because a high convergence rate increases the flux of seafloor into a subduction zone. Thus, there is directly more volume of ocean crust (either RAP or not) available to react. Hence, many of the subduction zones ringing the Pacific Ocean are overall more fertile than the slow Calabrian subduction zone, despite the fact that Calabria has a higher fraction of RAP being subducted (Figures 4 and 5). This correlation is likely slightly skewed for two reasons in our analysis. First, as we only consider the last 5 Ma, subduction zones with fast convergence rates are able to fully occupy the maximum pressure of the antigorite stability field. If our analysis was extended further back in time, the correlation may weaken slightly, as subduction zones with slower convergence rates would become fully populated. Second, the majority of present-day subduction occurs within the Pacific Ocean, while RAP at present-day is predominantly located within the Atlantic, Arctic and Indian ocean basins (Merdith et al., 2019). When these three ocean basins close in the future, we would expect a much higher RAP flux into subduction zones (e.g., Grevemeyer et al., 2018). Further back in Earth history, we hypothesize that during times of supercontinent tenure and breakup (e.g., 320–180 Ma for Pangea) there is a reduced flux of RAP being subducted; however, when supercontinents assemble and internal ocean basins close (e.g., Rheic, Iapetus Oceans, future Atlantic/Indian Ocean) we speculate that there will be an increased flux,

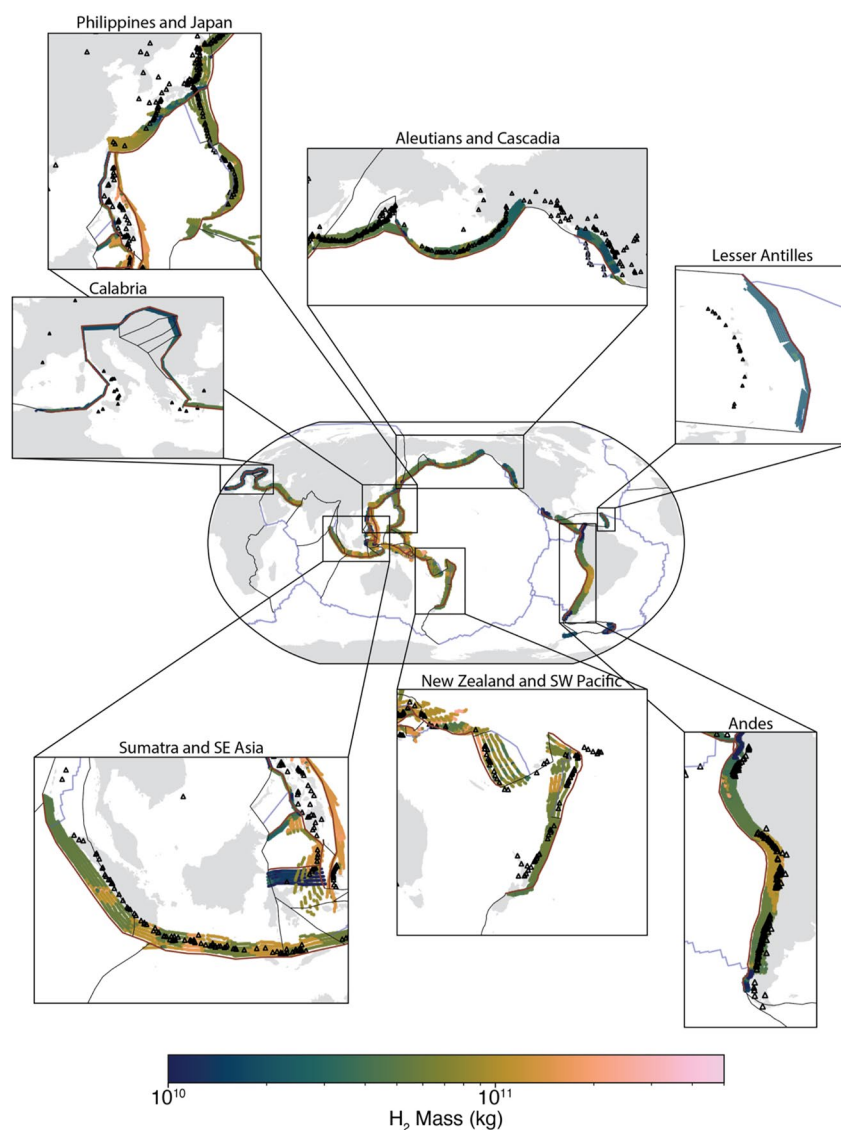


**Figure 5.** Modeled H<sub>2</sub> production through “slab-serpentinization” of residual abyssal peridotite over the last 5 Ma. The conversion to hydrogen includes all points currently subducted, including those that have passed through the antigorite stability field, and those that are yet to have passed through. Inserts show close-ups of some subduction zones discussed further in text. Holocene volcanoes are plotted on top from the Global Volcanism Project (2023). Global results of other parameters (e.g., fractional peridotite content, depth, dip etc. are available in Supporting Information S1). Results use a representative H<sub>2</sub> production value of 200 g per m<sup>3</sup> of reactant.

possibly up to several orders of magnitude on the global scale (e.g., Grevemeyer et al., 2018; Merdith et al., 2019) s, depending on the configuration of subduction zones. This hypothesis is contrary to hydrogen production at mid-ocean ridges, which is greatest as a supercontinent breaks-up (Merdith et al., 2020).

#### 4.2. Viability of Our Global Estimate

An increasing number of field-based, experimental, and theoretical studies have shown the possibility for H<sub>2</sub>-rich, strongly reduced fluids to form through serpentinization reactions in subduction zones (Ferrando et al., 2010; Sachan et al., 2007; Vitale Brovarone et al., 2017, 2020). However, global fluxes of deep H<sub>2</sub> related to this process are largely unconstrained. One way to assess the viability of our global estimate is to compare our volumetric fluxes to other similar fluxes within ocean basins, such as gross crustal production rates and H<sub>2</sub> fluxes within different oceanic environments.



Gross oceanic fluxes, including subduction flux and mid-ocean ridge flux, have been estimated in previous studies (e.g., East et al., 2019; Jarrard, 2003; Zahirovic et al., 2022). Our calculated volumetric flux of all subducted RAP within subduction zones ( $1.84 \bullet 10^6 \text{ km}^3$  per Ma) represents  $\sim 10\%$  of the total volume of subducted oceanic crust over the same time range ( $1.5 \bullet 10^7 \text{ km}^3$ , East et al., 2019). Our volume flux of subducted RAP is slightly lower than estimates for the total volumetric exhumation of the mantle at ridges (8%–14%, Worman et al., 2016) because the average spreading rate at present-day ridges is lower than the average spreading rate at the time of the creation of the crust currently being subducted.

There are few studies that look at serpentinization of RAP within subducting slabs, limiting our ability to make direct comparisons of our calculated  $\text{H}_2$  flux ( $4.2\text{--}24 \bullet 10^7 \text{ kg/a}$ ). One prior estimate by Vitale Brovarone et al., 2017 suggested that a minimum of 0.8 Mt/a (or  $8 \bullet 10^8 \text{ kg/a}$ ) of  $\text{H}_2$  could be generated globally through the serpentinization of  $0.21 \text{ km}^3/\text{a}$  of RAP in subduction zones. Their calculation was done using the present-day exhumation rate of peridotite at mid-ocean ridges as a proxy for equivalent subduction rates, and used a generalized stoichiometric reaction of pure olivine and water to serpentinite, brucite, magnetite and hydrogen after Berndt et al. (1996) and McCollom and Seewald (2001). If we use the same equation as Vitale Brovarone et al. (2017), but substitute our volumetric estimates of total subducted RAP over the last 5 Ma (averaging to be  $1.8 \text{ km}^3$  per annum), we calculate  $\sim 6.8 \text{ Mt/a}$  (or  $6.8 \bullet 10^9 \text{ kg/a}$ ) of  $\text{H}_2$  being formed. For both examples, the amount of hydrogen generated is greater than the approach using the data of Vitale Brovarone et al. (2020) described in our results earlier. This is because the balanced equation used by Vitale Brovarone et al. (2017) does not consider the changes in pressure-temperature and fluid composition that occur in a subduction zone.

Other environments where serpentinization occurs include mid-ocean ridges and the forearc mantle wedge (Hyndman & Peacock, 2003; Williams & Gubbins, 2019). Our calculated  $\text{H}_2$  flux over the past 5 Ma ( $4.2\text{--}24 \bullet 10^7 \text{ kg/a}$ ) is 3–4 orders of magnitude smaller than what is estimated to occur at present-day mid-ocean ridges (MOR,  $\sim 10^{11}\text{--}10^{12} \text{ kg/a}$ , see Figure 8 in Merdith et al. (2020) for a comparison of  $\text{H}_2$  values from MOR environments), but is at the upper end of a previous estimated range for  $\text{H}_2$  generation through serpentinization of the forearc mantle wedge, of  $9 \bullet 10^6$  to  $3 \bullet 10^8 \text{ kg/a}$  (Vitale Brovarone et al., 2020). If we follow the logic of Vitale Brovarone et al. (2020), who calculated their flux by water availability in the downgoing slab and assume that all water stored in the RAP-derived antigorite ( $\sim 15 \text{ wt}\%$ , and all RAP above the minimum stability of antigorite) from our study is liberated into the forearc mantle wedge, we estimate between  $3.4 \bullet 10^5$  and  $1.8 \bullet 10^7 \text{ kg/a}$  of  $\text{H}_2$  could be produced from mantle wedge serpentinization (one order of magnitude less).

Though not explicitly considered in our model, the deep hydration of the mantle lithosphere during subduction due to trench flexure (Ranero et al., 2003) is thought to induce extensive serpentinisation, with maximum estimates of  $\sim 30\%$ – $40\%$  serpentinisation (3–5 wt% hydration) of the first 30 km of lithospheric mantle (Carlson & Miller, 2003; Van Avendonk & Holbrook, 2011). Based on results from thermodynamic modelling and geophysical constraints, Faccenda (2014) proposed a more conservative estimate whereby on average 10% of the upper 5–10 km of the lithospheric mantle may be serpentinised ( $\sim 1.2 \text{ wt}\% \text{ H}_2\text{O}$ ). Using our gross subduction flux and assuming a hydrated upper mantle after Faccenda (2014) equates to a peridotite flux of  $13.5\text{--}27 \text{ km}^3$  per annum reacting with (sufficient) water to produce  $\sim 2.7\text{--}5.3 \bullet 10^9 \text{ kg}$  per annum of  $\text{H}_2$  (1–2 orders of magnitude greater than our estimate). There is, however, some large ambiguity about exactly how well hydrated the upper mantle is.

The existence of deep-faults from trench flexure is well established from seismic observation (e.g., Han et al., 2016; Ranero et al., 2003) and the resulting alteration is inferred from variations in seismic velocities (e.g., Carlson & Miller, 2003), but interconnecting alteration fronts between faults (into unfractured mantle) have been questioned based on rheological and seismic grounds (Hatakeyama et al., 2017; Korenaga, 2017; Miller et al., 2021). For instance, the Middle American Trench (MAT, outboard of Nicaragua) is thought to have the most hydrated mantle (due to trench flexure) of all subduction zones (e.g., Grevemeyer et al., 2018). Miller et al. (2021) proposed that the anisotropy observed within the trench rise of this subduction zone is best explained by discrete serpentinisation fronts, focussed around faults, without an interconnected reaction front. They suggest that at this subduction zone the bulk degree of serpentinisation and the corresponding hydration rates of the upper mantle (up to 10 km depth) are 6.1%–8.8%, corresponding to 0.60–0.87 wt%  $\text{H}_2\text{O}$ , respectively (Miller et al., 2021; Miller & Lizarralde, 2016). This estimate is roughly half that of Faccenda's (2014) global estimate and ca. 5–10 times our estimate from RAP, but, if propagated globally, would likely slightly over-estimate the budget due to the more abundant hydration at the MAT relative to other subduction zones.

Our estimates of volumetric peridotite subduction are a similar order of magnitude, but slightly lower than what is produced at mid-ocean ridges, which makes conceptual sense given that the majority of slow and ultraslow spreading ridges currently occur in ocean basins without extensive subduction zones (Merdith et al., 2020, e.g., 2019). A clear implication of this is that once the Atlantic and Arctic oceans begin closing, there is likely to be a much larger flux of RAP into global subduction systems (Grevemeyer et al., 2018). Our results are roughly equivalent (in terms of peridotite that reacts to form serpentinite and hydrogen) to the lower bounds of Faccenda (2014), or the upper bounds if the conclusions of Miller et al. (2021) are used. These results suggest that, globally, there could be a similar amount of RAP being subducted and serpentinitised as what is expected to occur due to trench flexure and upper-mantle hydration.

### 4.3. Ground-Truthing Our Model

Due to limitations in acquiring in situ measurements of active subduction zones, evaluation or ground truthing of our model is limited to comparing evidence of reactants (i.e., presence of RAP in a subduction zone *indicating possibility of slab-serpentinization*) or products (slab serpentinitization, hydrogen generation) in areas where our model suggests slab-serpentinization is occurring. Unfortunately, many of these comparisons are indirect and hampered by arc processes, the thick over-riding plate that alter original signals, biosphere, or through our inability to distinguish slab-serpentinization signatures from abyssal serpentinite, making it difficult to draw quantitative conclusions (Martin et al., 2020). Instead, methodological field-work and detailed petrography remain some of the best tools for evaluating slab-serpentinization in exhumed terranes (e.g., Vitale Brovarone et al., 2021) and consequently we infer our correlations as a conservative upper bound for slab serpentinitization.

The slab of the lesser Antilles subduction zone is Cretaceous in age, that was originally formed at an ultraslow-spreading ridge (Seton et al., 2012) and is currently converging at around 20 mm/a with a dip angle of 30°. IODP cruises that dredged and cored the ocean crust outboard of the trench have returned serpentinitized abyssal peridotite and residual abyssal peridotite, indicating that slow-spreading ocean crust is likely a major component of the oceanic crust and the slab (Klein et al., 2017). Seismic analysis of the Lesser Antilles slab suggests the presence of hydrated slow-spreading crust penetrating deeply (100 km) into the subduction zone (Bie et al., 2022; Paulatto et al., 2017). While a large and hydrated sediment budget may also account for the seismic anomalies, Paulatto et al. (2017) argue that the enrichment of isotopically heavy Mg in the lavas of Martinique Island is best explained by serpentinite-derived fluids from the subducting slab. Hick et al. (2022) came to a similar conclusion using seismic attenuation models, showing that the Lesser Antilles Island Arcs were likely formed through devolatilization of the subducting slab, with the pre-subduction tectonic history of the ocean slab imparting a strong control on the evolution of the mantle wedge and arc. Above the forearc mantle, fluid inclusions from the volcanic arc of the Lesser Antilles preserve strongly positive  $\delta^{11}\text{B}$  signatures, interpreted to be derived from the serpentinitization of the oceanic mantle (Cooper et al., 2020).

Though our model, in this subduction zone, only represents the upper 20–50 km of subducted slab in this region, the earlier subducting seafloor (i.e., subducted prior to 5 Ma) is likely also enriched to a similar degree in RAP (e.g., Merdith et al. 2019). We speculate that the upper 7 km of our modeled slab and the deeper slab both are comprised of roughly 15%–20% of RAP, indicating that an extensive serpentinitization front close to the slab-forearc contact is possible. Assessment of the veracity of this hypothesis will depend on the source of fluids that cause serpentinitization in the RAP; if they are derived metamorphically then they are unlikely to produce such a positive  $\delta^{11}\text{B}$  signature; however, if the fluids are sourced through, for example, further hydration during trench flexure, then they could produce a similar  $\delta^{11}\text{B}$  signature.

In addition to seismic imaging of slabs, ophiolites in active subduction zones may preserve either direct or indirect signatures substantiating slab-serpentinization and/or an underlying ultramafic subsurface. Direct evidence of slab-serpentinization has been presented for some ophiolites through the European Alps and Appalachians (Boutier et al., 2021; Scambelluri & Tonarini, 2012; Vitale Brovarone et al., 2020, 2021), a region our model suggests is rich in the subduction of RAP. In these ophiolites, a strongly positive  $\delta^{11}\text{B}$  signature is interpreted to be indicative of serpentinitization by seawater, rather than derived from the progressive dehydration of subducting oceanic crust, thus supporting serpentinitization of the downgoing slab (e.g., Scambelluri & Tonarini, 2012).

The Philippines archipelago straddles a complex set of tectonically dissected microplates sandwiched between the Manila and Philippine Trenches. The subsequent Zambales ophiolitic section, west from the Luzon Fault,

emplaced in the Oligocene to early Miocene, is famous for springs, several of which exhibit geochemical patterns indicative of active serpentinization in the ultramafic subsurface, rich in  $H_2$  and/or  $CH_4$  (Cardace et al., 2015). Though slightly older than the time region of analysis for our model, but probably representing a slightly older portion of the Philippines seafloor which subduction aborted, our results support the possible emplacement of extensive ultramafic bodies in this region, with the Philippine trench represented in our model much more abundant in RAP and subsequent  $H_2$  than other areas (e.g., Figures 3a and 3b). The nearest neighbor taxonomic affiliations of the microorganisms sampled in the springs obtained from  $^{16}S$  sequences show that the microbial communities are dominated by hydrogen oxidizers and archaeal methanogens genera. While not direct evidence of slab-serpentinization, the emplacement and subsequent serpentinization of residual abyssal peridotitic bodies in this region support our central proposition that RAP is subducting and could possibly undergo serpentinization in the slab.

#### 4.4. Implications for Subduction Systems and Hydrogen Generation

Our results have several broad implications for the nature of subduction systems and the generation of abiotic hydrogen (and methane). However, we stress that our model, while novel, is coarser than regional seismic tomography models and is not numerically coupled with either fluid, geodynamic, or petrological models depicting subduction zone processes (though this could be a future possibility). Here, we discuss our results with reference to general hypotheses about slab serpentinization processes.

Oceanic cold-deep seeps on active subduction zones are places where emissions of ambient-temperature fluids with high concentrations of  $CH_4$  seep from the lithosphere into the hydrosphere (Torres & Bohrmann, 2016). Many (but not all) of these seeps are found on margins poor in organic-rich sediments. For example, the compilation of cold-deep seeps offered by Torres and Bohrmann (2016) and also Suess (2014) show cold-deep seeps laying on both RAP-rich subduction zones (from our analysis, such as the European Alps down toward Turkey, the Antilles and Sumatra) and the organic carbon-poor subduction zones of Plank and Manning (2019), such as Cascadia and the Aleutians. In the absence of a clear organic origin, extensive serpentinization events leading to the generation of  $CH_4$  plumes could sustain these seeps. In particular, either serpentinized RAP (e.g., Meister et al., 2018; Sciarra et al., 2019) or where fracture zones subduct, allowing localized hydration of the upper mantle, could be a viable source of these seeps.

Causes of volcanic and arc gaps, segments of a continental arc that do not produce active volcanism despite ongoing evidence of subduction (McGeary et al., 1985), remain enigmatic. At present-day, the most predominant volcanic gaps occur along the South American Andean margin (Ramos, 1999) and in the Aleutians (Eberhart-Phillips and Christensen, 2006; the Denali Gap, e.g., Plafker & Berg, 1994). As continental arc volcanism is driven predominantly by partial melting in the mantle wedge and subducting slab (Gianni & Luján, 2021; Grove et al., 2012; Peacock, 1990), hypotheses to account for the absence of volcanism predominantly pertain to a combination of tectonic factors that essentially limit fluid generation. The most prominent hypotheses being flat slab subduction (dip angle  $<30^\circ$ , typically thought to occur because of slab buoyancy), which inhibits melt generation because the slab is unable to warm up sufficiently to induce melt, or thickened over-riding crust, where the mantle wedge remains cold and also inhibits the geotherm. Serpentinization, especially of RAP or the lithosphere in locations of thinned crust, are a possible intriguing piece in this puzzle, as they directly relate to processes that increase melt (due to abundance of water, possibly increasing volcanism (Grove et al., 2012)) and inhibit melt (through buoyancy, decreasing melt (Yang et al., 2020)).

To first order, our results indicate that serpentinization of the RAP is more strongly correlated with volcanism than with volcanic gaps (e.g., Figure 3, though we cannot omit that this could also correlate with serpentinite rich, slow-subducting lithosphere). This correlation is clearest in the Andean margin, where the one region with enriched RAP relative to the rest of the margin is beneath southern Peru and northern Chile, where there is abundant volcanism. In the northern volcanic gap along the Andean margin, our model suggests that a much smaller amount of RAP is likely being subducted (Figure 3). Along the Aleutian subduction zone, a similar transition is also observed, where low amounts of RAP are subducted in the NE corner of the subduction zone, where the Denali Gap occurs. However, these sections (Andean margin, Aleutians), while enriched relative to the rest of their margins, still contain far less RAP than other margins (Figure 4). Our overall results suggest that there could be some threshold in the flux of subducting RAP content that plays an important role in controlling the geometry and tectonic parameters of a subducting slab.

## 5. Implications and Conclusions

Recent studies have begun highlighting the nuance required to untangle subduction zone processes, in particular distinguishing the effect of localized slab features (e.g., fracture zones, thinned crust) and a heterogeneous slab composition on fluid generation and rheology of both the downgoing and overriding plate. Our analysis here couples discrete data sets, concretely linking the seafloor spreading history of present-day ocean basins to estimate the global potential of “slab-serpentinization” and resulting hydrogen generation. In particular, our results broadly support recent observations that reduced fluids can be generated in subduction zones (Vitale Brovarone et al., 2020), which have also been documented in the shallow forearc (e.g., Debret et al., 2022; Plümper et al., 2017). The framework we have constructed as part of this analysis can also be used to test different hypotheses about transport and interaction of volatiles and rocks from ocean basins into subduction zone settings (e.g., formation of magnetite as a product of slab-serpentinization and implications of deeper H<sub>2</sub> generation, transport of carbon, inter-relationships between slab age and subduction processes).

We identify two key controls on H<sub>2</sub> production within the serpentinite window in subducting slabs. First, H<sub>2</sub> production is dependent on determining how much raw material is available to undergo serpentinization. Our analysis identifies seafloor spreading rate at the time of crust formation as being the strongest tectonic control on possible H<sub>2</sub> production. Second, the P-T conditions of a subduction zone control the limit of the antigorite stability zone. The approach we have followed here allows us to estimate a minimum amount of hydrogen generated from subducting slabs, using volumes of RAP (connected directly to the seafloor spreading history of ocean basins) entering a subduction zone and determining the mass of RAP that is currently within, or has passed through, the antigorite stability zone. Our results suggest that up to 10<sup>8</sup> kg/a of hydrogen could be generated through slab-serpentinization across global subduction zones (3–4 orders of magnitude lower than at mid-ocean ridges), and we suggest that some well-identified volcanic gaps correlate with regions of less RAP being subducted.

## Data Availability Statement

All data and code used for this analysis are available at Merdith et al. (2023), as well as at [github.com/amer7632/Merdith2023\\_pgpSlabs\\_G3](https://github.com/amer7632/Merdith2023_pgpSlabs_G3) (where future updates will be stored).

## References

- Abers, G. A., van Keken, P. E., & Hacker, B. R. (2017). The cold and relatively dry nature of mantle forearcs in subduction zones. *Nature Geoscience*, 10(5), 333–337. <https://doi.org/10.1038/ngeo2922>
- Andreani, M., Muñoz, M., Marcaillou, C., & Delacour, A. (2013).  $\mu$ XANES study of iron redox state in serpentine during oceanic serpentinization. *Lithos*, 178, 70–83. <https://doi.org/10.1016/j.lithos.2013.04.008>
- Arai, S., Ishimaru, S., & Mizukami, T. (2012). Methane and propane micro-inclusions in olivine in titanoclinohumite-bearing dunites from the Sanbagawa high-P metamorphic belt, Japan: Hydrocarbon activity in a subduction zone and Ti mobility. *Earth and Planetary Science Letters*, 353–354, 1–11. <https://doi.org/10.1016/j.epsl.2012.07.043>
- Barbier, S., Huang, F., Andreani, M., Tao, R., Hao, J., Eleish, A., et al. (2020). A review of H<sub>2</sub>, CH<sub>4</sub>, and hydrocarbon formation in experimental serpentinization using network analysis. *Frontiers in Earth Science*, 8, 209. <https://doi.org/10.3389/feart.2020.00209>
- Barnes, I., O'Neil, J. R., & Trescases, J. J. (1978). Present day serpentinization in New Caledonia, Oman and Yugoslavia. *Geochimica et Cosmochimica Acta*, 42(1), 144–145. [https://doi.org/10.1016/0016-7037\(78\)90225-9](https://doi.org/10.1016/0016-7037(78)90225-9)
- Berndt, M. E., Allen, D. E., & Seyfried, W. E. (1996). Reduction of CO<sub>2</sub> during serpentinization of olivine at 300°C and 500 bar. *Geology*, 24(4), 351–354. [https://doi.org/10.1130/0091-7613\(1996\)024<0351:rocdso>2.3.co;2](https://doi.org/10.1130/0091-7613(1996)024<0351:rocdso>2.3.co;2)
- Bie, L., Hicks, S., Rietbrock, A., Goes, S., Collier, J., Rychert, C., et al. (2022). Imaging slab-transported fluids and their deep dehydration from seismic velocity tomography in the Lesser Antilles subduction zone. *Earth and Planetary Science Letters*, 586, 117535. <https://doi.org/10.1016/j.epsl.2022.117535>
- Blakely, R. J., Brocher, T. M., & Wells, R. E. (2005). Subduction-zone magnetic anomalies and implications for hydrated forearc mantle. *Geology*, 33(6), 445–448. <https://doi.org/10.1130/g21447.1>
- Bostock, M. G., Hyndman, R. D., Rondenay, S., & Peacock, S. M. (2002). An inverted continental Moho and serpentinization of the forearc mantle. *Nature*, 417(6888), 536–538. <https://doi.org/10.1038/417536a>
- Boutier, A., Vitale Brovarone, A., Martínez, I., Sissmann, O., & Mana, S. (2021). High-pressure serpentinization and abiotic methane formation in metaperidotite from the Appalachian subduction, northern Vermont. *Lithos*, 396–397, 106190. <https://doi.org/10.1016/j.lithos.2021.106190>
- Cannat, M., Fontaine, F., & Escartin, J. (2010). Serpentinization and associated hydrogen and methane fluxes at slow spreading ridges. In P. A. Rona, C. W. Devey, J. Dymont, & B. J. Murton (Eds.), *Diversity of hydrothermal systems on slow spreading ocean ridges, geophysical monograph series* (pp. 241–264). American Geophysical Union.
- Cardace, D., Meyer-Dombard, D. R., Woycheese, K. M., & Arcilla, C. A. (2015). Feasible metabolisms in high pH springs of the Philippines. *Frontiers in Microbiology*, 6, 10. <https://doi.org/10.3389/fmicb.2015.00010>
- Carlson, R. L., & Miller, D. J. (2003). Mantle wedge water contents estimated from seismic velocities in partially serpentinized peridotites. *Geophysical Research Letters*, 30(5), 1250. <https://doi.org/10.1029/2002GL016600>
- Charlou, J. L., Donval, J. P., Fouquet, Y., Jean-Baptiste, P., & Holm, N. (2002). Geochemistry of high H and CH vent fluids issuing from ultramafic rocks at the Rainbow hydrothermal field (36j14VN, MAR). *Chemical Geology*, 191(4), 345–359. [https://doi.org/10.1016/S0009-2541\(02\)00134-1](https://doi.org/10.1016/S0009-2541(02)00134-1)

## Acknowledgments

This research was supported by the Richard Lounsbery Foundation and MCSA Fellowship NEOEARTH, project 893615 and ERC project Deep Seep 864045. Figures were made using scientific colour maps (Crameri, 2018). K. Wong is thanked for assistance in tidying and checking the model, and Nadia Malaspina, an anonymous reviewer and Marie Edmonds are thanked for their comments and editorial handling.



- Cooper, G. F., Macpherson, C. G., Blundy, J. D., Maunder, B., Allen, R. W., Goes, S., et al. (2020). Author correction: Variable water input controls evolution of the Lesser Antilles volcanic arc. *Nature*, 584(7822), E36. <https://doi.org/10.1038/s41586-020-2582-4>
- Cramer, F. (2018). Scientific colour-maps.
- Debret, B., Ménez, B., Walter, B., Bouquerel, H., Bouilhol, P., Mattioli, N., et al. (2022). High-pressure synthesis and storage of solid organic compounds in active subduction zones. *Science Advances*, 8(37), eabo2397. <https://doi.org/10.1126/sciadv.abo2397>
- Debret, B., & Sverjensky, D. A. (2017). Highly oxidising fluids generated during serpentinite breakdown in subduction zones. *Scientific Reports*, 7(1), 10351. <https://doi.org/10.1038/s41598-017-09626-y>
- East, M., Müller, R. D., Williams, S., Zahirovic, S., & Heine, C. (2019). Subduction history reveals Cretaceous slab superflux as a possible cause for the mid-Cretaceous plume pulse and superswell events. *Gondwana Research*.
- Eberhart-Phillips, D., Christensen, D. H., Brocher, T. M., Hansen, R., Ruppert, N. A., Haeussler, P. J., & Abers, G. A. (2006). Imaging the transition from Aleutian subduction to Yakutat collision in central Alaska, with local earthquakes and active source data. *Journal of Geophysical Research*, 111(B11), B11303. <https://doi.org/10.1029/2005jb004240>
- Evans, B. W. (2004). The serpentinite multisystem revisited: Chrysotile is metastable. *International Geology Review*, 46(6), 479–506. <https://doi.org/10.2747/0020-6814.46.6.479>
- Faccenda, M. (2014). Water in the slab: A trilogy. *Tectonophysics*, 614, 1–30. <https://doi.org/10.1016/j.tecto.2013.12.020>
- Ferrando, S., Frezzotti, M. L., Orione, P., Conte, R. C., & Compagnoni, R. (2010). Late-alpine rodingitization in the Bellecombe meta-ophiolites (Aosta valley, Italian western Alps): Evidence from mineral assemblages and serpentinitization-derived H<sub>2</sub>-bearing brine. *International Geology Review*, 52(10–12), 1220–1243. <https://doi.org/10.1080/00206810903557761>
- Fryer, P. (1996). Evolution of the Mariana convergent plate margin system. *Review of Geophysics*, 34(1), 89–125. <https://doi.org/10.1029/95RG03476>
- Galvez, M. E., Martinez, I., Beyssac, O., Benzerara, K., Agrinier, P., & Assayag, N. (2013). Metasomatism and graphite formation at a lithological interface in Malaspina (Alpine Corsica, France). *Contributions to Mineralogy and Petrology*, 166(6), 1687–1708. <https://doi.org/10.1007/s00410-013-0949-3>
- Gianni, G. M., & Luján, S. P. (2021). Geodynamic controls on magmatic arc migration and quiescence. *Earth-Science Reviews*, 218, 103676. <https://doi.org/10.1016/j.earscirev.2021.103676>
- Global Volcanism Program. (2023). [Database] volcanoes of the world (v. 5.1.1; 17 August 2023). Distributed by Smithsonian Institution, compiled by Venzke, E. <https://doi.org/10.5479/si.GVP.VOTW5-2023.5.1>
- Grevemeyer, I., Ranero, C. R., & Ivandic, M. (2018). Structure of oceanic crust and serpentinitization at subduction trenches. *Geosphere*, 14(2), 395–418. <https://doi.org/10.1130/ges01537.1>
- Grove, T. L., Till, C. B., & Krawczynski, M. J. (2012). The role of H<sub>2</sub>O in subduction zone magmatism. *Annual Review of Earth and Planetary Sciences*, 40(1), 413–439. <https://doi.org/10.1146/annurev-earth-042711-105310>
- Han, S., Carbotte, S. M., Canales, J. P., Nedimović, M. R., Carton, H., Gibson, J. C., & Horning, G. W. (2016). Seismic reflection imaging of the Juan de Fuca plate from ridge to trench: New constraints on the distribution of faulting and evolution of the crust prior to subduction. *Journal of Geophysical Research: Solid Earth*, 121(3), 1849–1872. <https://doi.org/10.1002/2015jb012416>
- Harmon, N., Rychert, C., Collier, J., Henstock, T., van Hunen, J., & Wilkinson, J. J. (2019). Mapping geologic features onto subducted slabs. *Geophysical Journal International*, 219(2), 725–733. <https://doi.org/10.1093/gji/ggz290>
- Hatakeyama, K., Katayama, I., Hirauchi, K.-I., & Michibayashi, K. (2017). Mantle hydration along outer-rise faults inferred from serpentinite permeability. *Scientific Reports*, 7(1), 13870. <https://doi.org/10.1038/s41598-017-14309-9>
- Hayes, G. P., Moore, G. L., Portner, D. E., Hearne, M., Flamme, H., Furtney, M., & Smoczyk, G. M. (2018). Slab2, a comprehensive subduction zone geometry model. *Science*, 362(6410), 58–61. <https://doi.org/10.1126/science.aat4723>
- Hicks, S. P., Bie, L., Rychert, C., Harmon, N., Goes, S., Rietbrock, A., et al. (2022). Slab to back-arc to arc: Fluid and melt pathways through the mantle wedge beneath the lesser Antilles.
- Hu, J., & Gurnis, M. (2020). Subduction duration and slab dip. *Geochemistry, Geophysics, Geosystems*, 21(4), e2019GC008862. <https://doi.org/10.1029/2019gc008862>
- Huang, F., Daniel, I., Cardon, H., Montagnac, G., & Sverjensky, D. A. (2017). Immiscible hydrocarbon fluids in the deep carbon cycle. *Nature Communications*, 8(1), 15798. <https://doi.org/10.1038/ncomms15798>
- Hyndman, R. D., & Peacock, S. M. (2003). Serpentinization of the Forearc mantle. *Earth and Planetary Science Letters*, 212(3–4), 417–432. [https://doi.org/10.1016/s0012-821x\(03\)00263-2](https://doi.org/10.1016/s0012-821x(03)00263-2)
- Jacob, J., Dymant, J., & Yatheesh, V. (2014). Revisiting the structure, age, and evolution of the Wharton basin to better understand subduction under Indonesia. *Journal of Geophysical Research: Solid Earth*, 119(1), 169–190. <https://doi.org/10.1002/2013jb010285>
- Janecky, D. R., & Seyfried, W. E. (1986). Hydrothermal serpentinization of peridotite within the oceanic crust: Experimental investigations of mineralogy and major element chemistry. *Geochimica et Cosmochimica Acta*, 50(7), 1357–1378. [https://doi.org/10.1016/0016-7037\(86\)90311-x](https://doi.org/10.1016/0016-7037(86)90311-x)
- Jarrard, R. D. (2003). Subduction fluxes of water, carbon dioxide, chlorine, and potassium. *Geochemistry, Geophysics, Geosystems*, 4(5), 8905. <https://doi.org/10.1029/2002GC000392>
- Kelley, D. S., Karson, J. A., Früh-Green, G. L., Yoerger, D. R., Shank, T. M., Butterfield, D. A., et al. (2005). A serpentinite-hosted ecosystem: The Lost City hydrothermal field. *Science*, 307(5714), 1428–1434. <https://doi.org/10.1126/science.1102556>
- Klein, F., Marschall, H. R., Bowring, S. A., Humphris, S. E., & Horning, G. (2017). Mid-ocean ridge serpentinite in the Puerto Rico trench: From seafloor spreading to subduction. *Journal of Petrology*, 58(9), 1729–1754. <https://doi.org/10.1093/ptrology/egx071>
- Korenaga, J. (2017). On the extent of mantle hydration caused by plate bending. *Earth and Planetary Science Letters*, 457, 1–9. <https://doi.org/10.1016/j.epsl.2016.10.011>
- Kutcherov, V. G., Dmitrievsky, A. N., Ivanov, K. S., & Serovskii, A. Y. (2020). The deep hydrocarbon cycle: From subduction to mantle upwelling. *Doklady Earth Sciences*, 492(1), 338–341. <https://doi.org/10.1134/s1028334x20050098>
- Leong, J. A. M., Howells, A. E., Robinson, K. J., Cox, A., Debes, R. V., II, Fecteau, K., et al. (2021). Theoretical predictions versus environmental observations on serpentinitization fluids: Lessons from the samail ophiolite in Oman. *Journal of Geophysical Research: Solid Earth*, 126(4), e2020JB020756. <https://doi.org/10.1029/2020jb020756>
- Leong, J. A. M., & Shock, E. L. (2020). Thermodynamic constraints on the geochemistry of low-temperature, continental, serpentinitization-generated fluids. *American Journal of Science*, 320(3), 185–235. <https://doi.org/10.2475/03.2020.01>
- Liu, Z., Perez-Gussinye, M., García-Pintado, J., Mezri, L., & Bach, W. (2023). Mantle serpentinitization and associated hydrogen flux at North Atlantic magma-poor rifted margins. *Geology*, 51(3), 284–289. <https://doi.org/10.1130/G50722.1>
- Malaspina, N., Campione, M., Tumiati, S., Murri, M., Fumagalli, P., Cerantola, V., et al. (2023). Epitactic magnetite growth in fluid inclusions as driving force for olivine oxidation coupled with hydrogen production at high pressure. *Chemical Geology*, 629, 121495. <https://doi.org/10.1016/j.chemgeo.2023.121495>

- Malvoisin, B., Chopin, C., Brunet, F., & Galvez, M. E. (2011). Low-temperature wollastonite formed by carbonate reduction: A marker of serpentinite redox conditions. *Journal of Petrology*, 53(1), 159–176. <https://doi.org/10.1093/ptrology/egr060>
- Manning, C. E., Shock, E. L., & Sverjensky, D. A. (2013). The chemistry of carbon in aqueous fluids at crustal and upper-mantle conditions: Experimental and theoretical constraints. *Reviews in Mineralogy and Geochemistry*, 75(1), 109–148. <https://doi.org/10.2138/rmg.2013.75.5>
- Martin, C., Flores, K. E., Vitale Brovarone, A., Angiboust, S., & Harlow, G. E. (2020). Deep mantle serpentinization in subduction zones: Insight from in situ B isotopes in slab and mantle wedge serpentinites. *Chemical Geology*, 545, 119637. <https://doi.org/10.1016/j.chemgeo.2020.119637>
- Mather, B. R., Müller, R. D., Alfonso, C. P., Seton, M., & Wright, N. M. (2023). Kimberlite eruptions driven by slab flux and subduction angle. *Scientific Reports*, 13(1), 9216. <https://doi.org/10.1038/s41598-023-36250-w>
- Maurice, J., Bolfan-Casanova, N., Demouchy, S., Chauvigne, P., Schiavi, F., & Debret, B. (2020). The intrinsic nature of antigorite breakdown at 3 GPa: Experimental constraints on redox conditions of serpentinite dehydration in subduction zones. *Contributions to Mineralogy and Petrology*, 175(10), 94. <https://doi.org/10.1007/s00410-020-01731-y>
- McCollom, T. M., & Seewald, J. S. (2001). A reassessment of the potential for reduction of dissolved CO<sub>2</sub> to hydrocarbons during serpentinization of olivine. *Geochimica et Cosmochimica Acta*, 65(21), 3769–3778. [https://doi.org/10.1016/S0016-7037\(01\)00655-x](https://doi.org/10.1016/S0016-7037(01)00655-x)
- McGeary, S., Nur, A., & Ben-Avraham, Z. (1985). Spatial gaps in arc volcanism: The effect of collision or subduction of oceanic plateaus. *Tectonophysics*, 119(1–4), 195–221. [https://doi.org/10.1016/0040-1951\(85\)90039-3](https://doi.org/10.1016/0040-1951(85)90039-3)
- McGirr, R., Seton, M., & Williams, S. (2021). Kinematic and geodynamic evolution of the Isthmus of Panama region: Implications for central American Seaway closure. *Bulletin - American Association for the History of Nursing*, 133(3–4), 867–884. <https://doi.org/10.1130/b35595.1>
- Meister, P., Wiedling, J., Lott, C., Bach, W., Kuhfuß, H., Wegener, G., et al. (2018). Anaerobic methane oxidation inducing carbonate precipitation at abiogenic methane seeps in the Tuscan archipelago (Italy). *PLoS One*, 13(12), e0207305. <https://doi.org/10.1371/journal.pone.0207305>
- Merdith, A. S., Atkins, S. E., & Tetley, M. G. (2019). Tectonic controls on carbon and serpentinite storage in subducted upper oceanic lithosphere for the past 320 Ma. *Frontiers of Earth Science in China*, 7, 332. <https://doi.org/10.3389/feart.2019.00332>
- Merdith, A. S., Daniel, I., Sverjensky, D., Andreani, M., Mather, B., Williams, S., & Vitale Brovarone, A. (2023). Global hydrogen production during high-pressure serpentinization of subducting slabs—Dataset (1.0) [Dataset]. Zenodo. <https://doi.org/10.5281/zenodo.7728896>
- Merdith, A. S., Del Real, P. G., Daniel, I., Andreani, M., Wright, N. M., & Coltice, N. (2020). Pulsated global hydrogen and methane flux at mid-ocean ridges driven by Pangea breakup. *Geochemistry, Geophysics, Geosystems*, 21(4), e2019GC008869. <https://doi.org/10.1029/2019gc008869>
- Miller, H. M., Matter, J. M., Kelemen, P., Ellison, E. T., Conrad, M. E., Fierer, N., et al. (2016). Modern water/rock reactions in Oman hyperalkaline peridotite aquifers and implications for microbial habitability. *Geochimica et Cosmochimica Acta*, 179, 217–241. <https://doi.org/10.1016/j.gca.2016.01.033>
- Miller, N. C., & Lizarralde, D. (2016). Finite-frequency wave propagation through outer rise fault zones and seismic measurements of upper mantle hydration. *Geophysical Research Letters*, 43(15), 7982–7990. <https://doi.org/10.1002/2016gl070083>
- Miller, N. C., Lizarralde, D., Collins, J. A., Holbrook, W. S., & Van Avendonk, H. J. A. (2021). Limited mantle hydration by bending faults at the Middle America trench. *Journal of Geophysical Research: Solid Earth*, 126(1), e2020JB020982. <https://doi.org/10.1029/2020jb020982>
- Mottl, M. J., Komor, S. C., Fryer, P., & Moyer, C. L. (2003). Deep-slab fluids fuel extremophilic Archaea on a Mariana Forearc serpentinite mud volcano: Ocean Drilling Program Leg 195. *Geochemistry, Geophysics, Geosystems*, 4(11), 9009. <https://doi.org/10.1029/2003gc000588>
- Müller, R. D., Seton, M., Zahirovic, S., Williams, S. E., Matthews, K. J., Wright, N. M., et al. (2016). Ocean basin evolution and global-scale plate reorganization events since Pangea breakup. *Annual Review of Earth and Planetary Sciences*, 44(1), 107–138. <https://doi.org/10.1146/annurev-earth-060115-012211>
- Ohara, Y., Reagan, M. K., Fujikura, K., Watanabe, H., Michibayashi, K., Ishii, T., et al. (2012). A serpentinite-hosted ecosystem in the southern Mariana Forearc. *Proceedings of the National Academy of Sciences of the United States of America*, 109(8), 2831–2835. <https://doi.org/10.1073/pnas.1112005109>
- Padrón-Navarta, J. A., López Sánchez-Vizcaíno, V., Menzel, M. D., Gómez-Pugnaire, M. T., & Garrido, C. J. (2023). Mantle wedge oxidation from deserpentinization modulated by sediment-derived fluids. *Nature Geoscience*, 16(3), 268–275. <https://doi.org/10.1038/s41561-023-01127-0>
- Parkinson, I. J., & Arculus, R. J. (1999). The redox state of subduction zones: Insights from arc-peridotites. *Chemical Geology*, 160(4), 409–423. [https://doi.org/10.1016/S0009-2541\(99\)00110-2](https://doi.org/10.1016/S0009-2541(99)00110-2)
- Paulatto, M., Laïgle, M., Galve, A., Charvis, P., Sapin, M., Bayraktci, G., et al. (2017). Dehydration of subducting slow-spread oceanic lithosphere in the Lesser Antilles. *Nature Communications*, 8(1), 15980. <https://doi.org/10.1038/ncomms15980>
- Peacock, S. A. (1990). Fluid processes in subduction zones. *Science*, 248(4953), 329–337. <https://doi.org/10.1126/science.248.4953.329>
- Piccoli, F., Hermann, J., Pettke, T., Connolly, J. A. D., Kempf, E. D., & Vieira Duarte, J. F. (2019). Subducting serpentinites release reduced, not oxidized, aqueous fluids. *Scientific Reports*, 9(1), 19573. <https://doi.org/10.1038/s41598-019-55944-8>
- Plafker, G., & Berg, H. C. (1994). Overview of the geology and tectonic evolution of Alaska. <https://doi.org/10.1130/DNAG-GNA-G1.989>
- Plank, T., & Manning, C. E. (2019). Subducting carbon. *Nature*, 574(7778), 343–352. <https://doi.org/10.1038/s41586-019-1643-z>
- Plümpner, O., King, H. E., Geisler, T., Liu, Y., Pabst, S., Savov, I. P., et al. (2017). Subduction zone forearc serpentinites as incubators for deep microbial life. *Proceedings of the National Academy of Sciences of the United States of America*, 114(17), 4324–4329. <https://doi.org/10.1073/pnas.1612147114>
- Ramos, V. A. (1999). Plate tectonic setting of the Andean Cordillera. *Episodes*, 22(3), 183–190. <https://doi.org/10.18814/epiugs/1999v22i3/005>
- Ranero, C. R., Morgan, J. P., McIntosh, K., & Reichert, C. (2003). Bending-related faulting and mantle serpentinization at the Middle America trench. *Nature*, 425(6956), 367–373. <https://doi.org/10.1038/nature01961>
- Rogers, T. J., Buongiorno, J., Jessen, G. L., Schrenk, M. O., Fordyce, J. A., de Moor, J. M., et al. (2023). Chemolithoautotroph distributions across the subsurface of a convergent margin. *ISME Journal*, 17(1), 140–150. <https://doi.org/10.1038/s41396-022-01331-7>
- Sachan, H. K., Mukherjee, B. K., & Bodnar, R. J. (2007). Preservation of methane generated during serpentinization of upper mantle rocks: Evidence from fluid inclusions in the Nidar ophiolite, Indus Suture Zone, Ladakh (India). *Earth and Planetary Science Letters*, 257(1–2), 47–59. <https://doi.org/10.1016/j.epsl.2007.02.023>
- Sánchez-Murillo, R., Gazel, E., Schwarzenbach, E. M., Crespo-Medina, M., Schrenk, M. O., Boll, J., & Gill, B. C. (2014). Geochemical evidence for active tropical serpentinization in the Santa Elena Ophiolite, Costa Rica: An analog of a humid early Earth? *Geochemistry, Geophysics, Geosystems*, 15(5), 1783–1800. <https://doi.org/10.1002/2013gc005213>
- Scambelluri, M., & Tonarini, S. (2012). Boron isotope evidence for shallow fluid transfer across subduction zones by serpentinized mantle. *Geology*, 40(10), 907–910. <https://doi.org/10.1130/g33233.1>
- Schmidt, M. W., & Poli, S. (2013). Devolatilization during subduction. In *Treatise on geochemistry* (pp. 669–701). Elsevier.
- Schwartz, S., Guillot, S., Reynard, B., Lafay, R., Debret, B., Nicollet, C., et al. (2013). Pressure–temperature estimates of the lizardite/antigorite transition in high pressure serpentinites. *Lithos*, 178, 197–210. <https://doi.org/10.1016/j.lithos.2012.11.023>
- Sciarrà, A., Saroni, A., Etiope, G., Coltorti, M., Mazzarini, F., Lott, C., et al. (2019). Shallow submarine seep of abiotic methane from serpentinized peridotite off the Island of Elba, Italy. *Applied Geochemistry*, 100, 1–7. <https://doi.org/10.1016/j.apgeochem.2018.10.025>

- Seton, M., Müller, R. D., Zahirovic, S., Gaina, C., Torsvik, T., Shephard, G., et al. (2012). Global continental and ocean basin reconstructions since 200 Ma. *Earth-Science Reviews*, *113*(3–4), 212–270. <https://doi.org/10.1016/j.earscirev.2012.03.002>
- Seton, M., Müller, R. D., Zahirovic, S., Williams, S., Wright, N. M., Cannon, J., et al. (2020). A global data set of present-day oceanic crustal age and seafloor spreading parameters. *Geochemistry: Exploration, Environment, Analysis*, *21*(10). <https://doi.org/10.1029/2020gc009214>
- Seton, M., Williams, S. E., Domeier, M., Collins, A. S., & Sigloch, K. (2023). Deconstructing plate tectonic reconstructions. *Nature Reviews Earth & Environment*, *4*(3), 1–20. <https://doi.org/10.1038/s43017-022-00384-8>
- Suess, E. (2014). Marine cold seeps and their manifestations: Geological control, biogeochemical criteria and environmental conditions. *Geologische Rundschau*, *103*(7), 1889–1916. <https://doi.org/10.1007/s00531-014-1010-0>
- Sverjensky, D., & Daniel, I. (2020). The changing character of carbon in fluids with pressure: Organic geochemistry of Earth's upper mantle fluids. *Carbon in Earth's Interior*.
- Syracuse, E. M., van Keken, P. E., & Abers, G. A. (2010). The global range of subduction zone thermal models. *Physics of the Earth and Planetary Interiors*, *183*(1–2), 73–90. <https://doi.org/10.1016/j.pepi.2010.02.004>
- Tao, R., Zhang, L., Tian, M., Zhu, J., Liu, X., Liu, J., et al. (2018). Formation of abiogenic hydrocarbon from reduction of carbonate in subduction zones: Constraints from petrological observation and experimental simulation. *Geochimica et Cosmochimica Acta*, *239*, 390–408. <https://doi.org/10.1016/j.gca.2018.08.008>
- Torres, M. E., & Bohrmann, G. (2016). Cold seeps. In J. Harff, M. Meschede, S. Petersen, & J. Thiede (Eds.), *Encyclopedia of marine geosciences, encyclopedia of Earth sciences series* (pp. 117–122). Springer Netherlands.
- Tucholke, B. E., & Lin, J. (1994). A geological model for the structure of ridge segments in slow spreading ocean crust. *Journal of Geophysical Research*, *99*(B6), 11937–11958. <https://doi.org/10.1029/94jb00338>
- Tumiati, S., & Malaspina, N. (2019). Redox processes and the role of carbon-bearing volatiles from the slab–mantle interface to the mantle wedge. *Journal of the Geological Society*, *176*(2), 388–397. <https://doi.org/10.1144/jgs2018-046>
- Ulmer, P., & Trommsdorff, V. (1995). Serpentine stability to mantle depths and subduction-related magmatism. *Science*, *268*(5212), 858–861. <https://doi.org/10.1126/science.268.5212.858>
- Van Avendonk, H. J. A., & Holbrook, W. S. (2011). *Structure and serpentinization of the subducting Cocos plate offshore Nicaragua and Costa Rica*. Exploration, Environment, Analysis. <https://doi.org/10.1029/2011GC003592>
- van Keken, P. E., Hacker, B. R., Syracuse, E. M., & Abers, G. A. (2011). Subduction factory: 4. Depth-Dependent flux of H<sub>2</sub>O from subducting slabs worldwide. *Journal of Geophysical Research*, *116*(B1), B01401. <https://doi.org/10.1029/2010jb007922>
- Vitale Brovarone, A., Martinez, I., Elmaleh, A., Compagnoni, R., Chaduteau, C., Ferraris, C., & Esteve, I. (2017). Massive production of abiogenic methane during subduction evidenced in metamorphosed opihcarbonates from the Italian Alps. *Nature Communications*, *8*(1), 14134. <https://doi.org/10.1038/ncomms14134>
- Vitale Brovarone, A., Piccoli, F., Frasca, G., & Giuntoli, F. (2021). Fresh, Pseudotachylite-bearing mantle peridotites from the Lawsonite Eclogite-Facies San Petrone unit, Alpine Corsica. *Ophioliti*, *46*. <https://doi.org/10.4454/ofioliti.v46i2.545>
- Vitale Brovarone, A., Sverjensky, D. A., Piccoli, F., Ressico, F., Giovannelli, D., & Daniel, I. (2020). Subduction hides high-pressure sources of energy that may feed the deep subsurface biosphere. *Nature Communications*, *11*(1), 3880. <https://doi.org/10.1038/s41467-020-17342-x>
- Williams, S. E., & Gubbins, D. (2019). Origin of long-wavelength magnetic anomalies at subduction zones. *Journal of Geophysical Research: Solid Earth*, *124*(9), 9457–9473. <https://doi.org/10.1029/2019jb017479>
- Worman, S. L., Pratson, L. F., Karson, J. A., & Klein, E. M. (2016). Global rate and distribution of H<sub>2</sub> gas produced by serpentinization within oceanic lithosphere: H<sub>2</sub> formation in ocean lithosphere. *Geophysical Research Letters*, *43*(12), 6435–6443. <https://doi.org/10.1002/2016gl069066>
- Yang, J., Lu, G., Liu, T., Li, Y., & Wang, K. (2020). *Amagmatic subduction produced by mantle serpentinization and oceanic crust delamination*. Geophysical.
- Zahirovic, S., Eleish, A., Doss, S., Pall, J., Cannon, J., Pistone, M., et al. (2022). Subduction and carbonate platform interactions. *Geoscience Data Journal*, *9*(2), 371–383. <https://doi.org/10.1002/gdj3.146>

## References From the Supporting Information

- Bonnemains, D., Carlut, J., Escartín, J., Mével, C., Andreani, M., & Debret, B. (2016). Magnetic signatures of serpentinization at ophiolite complexes. *Geochemistry, Geophysics, Geosystems*, *17*(8), 2969–2986. <https://doi.org/10.1002/2016gc006321>
- Cannat, M., Mevel, C., Maia, M., Deplus, C., Durand, C., Gente, P., et al. (1995). Thin crust, ultramafic exposures, and rugged faulting patterns at the mid-Atlantic ridge (22°–24°N). *Geology*, *23*(1), 49–52. [https://doi.org/10.1130/0091-7613\(1995\)023<0049:tcuear>2.3.co;2](https://doi.org/10.1130/0091-7613(1995)023<0049:tcuear>2.3.co;2)
- Cannat, M., Sauter, D., Lavier, L., Bickert, M., Momoh, E., & Leroy, S. (2019). On spreading modes and magma supply at slow and ultraslow mid-ocean ridges. *Earth and Planetary Science Letters*, *519*(August), 223–233. <https://doi.org/10.1016/j.epsl.2019.05.012>
- Gurnis, M., Turner, M., Zahirovic, S., DiCaprio, L., Spasojevic, S., Müller, R. D., et al. (2012). Plate tectonic reconstructions with continuously closing plates. *Computers & Geosciences*, *38*(1), 35–42. <https://doi.org/10.1016/j.cageo.2011.04.014>
- Klein, F., Bach, W., Humphris, S. E., Kahl, W.-A., Jöns, N., Moskowicz, B., & Berquó, T. S. (2014). Magnetite in seafloor serpentinite—Some like it hot. *Geology*, *42*(2), 135–138. <https://doi.org/10.1130/g35068.1>
- Oufi, O. (2002). Magnetic properties of variably serpentinized abyssal peridotites. *Journal of Geophysical Research*, *107*(B5), 381. <https://doi.org/10.1029/2001jb000549>
- Syracuse, E. M., & Abers, G. A. (2006). Global compilation of variations in slab depth beneath arc volcanoes and implications. *Geochemistry, Geophysics, Geosystems*, *7*(5), Q05017. <https://doi.org/10.1029/2005gc001045>
- Toft, P. B., Arkani-Hamed, J., & Haggerty, S. E. (1990). The effects of serpentinization on density and magnetic susceptibility: A petrophysical model. *Physics of the Earth and Planetary Interiors*, *65*(1), 137–157. [https://doi.org/10.1016/0031-9201\(90\)90082-9](https://doi.org/10.1016/0031-9201(90)90082-9)
- Tucholke, B. E., Lin, J., & Kleinrock, M. C. (1998). Megamullions and mullion structure defining oceanic metamorphic core complexes on the mid-Atlantic ridge. *Journal of Geophysical Research*, *103*(B5), 9857–9866. <https://doi.org/10.1029/98jb00167>